Structural Engineering and Mechanics, *Vol. 63, No. 6 (2017) 743-750*
DOI: https://doi.org/10.12989/sem.2017.63.6.743

Spurious mode distinguish by eigensystem realization algorithm with improved stabilization diagram

Chun-Xu Qu[1,2a], Ting-Hua Yi[*1], Xiao-Mei Yang[1b] and Hong-Nan Li[1c]

[1]*School of Civil Engineering, Dalian University of Technology, Dalian, 116024, China*
[2]*State Key Laboratory of Building Safety and Built Environment, Beijing, 100013, China*

(Received November 16, 2016, Revised April 13, 2017, Accepted May 1, 2017)

Abstract. Modal parameter identification plays a key role in the structural health monitoring (SHM) for civil engineering. Eigensystem realization algorithm (ERA) is one of the most popular identification methods. However, the complex environment around civil structures can introduce the noises into the measurement from SHM system. The spurious modes would be generated due to the noises during ERA process, which are usually ignored and be recognized as physical modes. This paper proposes an improved stabilization diagram method in ERA to distinguish the spurious modes. First, it is proved that the ERA can be performed by any two Hankel matrices with one time step shift. The effect of noises on the eigenvalues of structure is illustrated when the choice of two Hankel matrices with one time step shift is different. Then, a moving data diagram is proposed to combine the traditional stabilization diagram to form the improved stabilization diagram method. The moving data diagram shows the mode variation along the different choice of Hankel matrices, which indicates whether the mode is spurious or not. The traditional stabilization diagram helps to determine the concerned truncated order before moving data diagram is implemented. Finally, the proposed method is proved through a numerical example. The results show that the proposed method can distinguish the spurious modes.

Keywords: eigensystem realization algorithm (ERA); spurious mode; stabilization diagram; Hankel matrix; singular value decomposition (SVD)

1. Introduction

The modal identification for civil engineering has attracted many researchers, which can be used for evaluation of structural safety (Lei *et al*. 2014), sensor optimal placement (Yi *et al*. 2011, Yi *et al*. 2012), structural response estimation and model updating. Li *et al*. (2016) proposed a new method for bilinear structural response estimation by bilinear modal shapes. Chen and Maung (2014) presented an iterative solution procedure for model updating based on dynamic perturbation method, which didn't need an optimization method and was improved to obtain stable solutions based on Tikhonov solution. Au and Zhang proposed a two-stage approach to identify the most probable values of the modal parameters and update the model parameters according to ambient vibration data based on Bayesian theory (Au and Zhang 2016, Zhang and Au 2016). For the above application of modal identification, most of these methods are based on the assumptions that the ambient excitation is white, such as stochastic subspace identification method (SSI) (Van Overschee and De Moor 2012). Eigensystem realization algorithm (ERA) (Juang and Pappa 1985) is performed by the pulse free responses, which can be achieved through the natural excitation technique (NExT) (James *et al*. 1995) or the random decrement method (RDT) (Ibraham 2001) from ambient excitation with white property. Due to the complicate environment of practical engineering, the assumptions are usually conflicted, which causes that the measurement is not compatible with the response formula in the identification method. The difference can be recognized as noises. And the practical noises do exist in measurement. The noises can introduce the spurious modes, which would lead to the inaccuracy of structural modes to SHM, structural safety evaluation and so on. Therefore, the spurious modes introduced by noises in the structural responses should be investigated and distinguished.

In the Hankel matrix based identification method, the noises in the measurement would be added into Hankel matrix. Then Hankel matrix with the additive noise matrix would be decomposed by the singular value decomposition (SVD) technique. The singular values of noises are not small enough, which are usually closed to some real singular values of the Hankel matrix. Therefore, the order of singular value matrix or the Hankel matrix is hard to be determined or truncated, which causes the spurious mode in the following eigenvalue calculation from the identified state matrix. It is obvious that the truncated order is the root cause. Up to now, the methods to determine the truncated order are almost classified into three aspects: the stabilization diagram (Peeters and Roeck 2001), the treatment of singular values and eigenvalues or

∗Corresponding author, Professor
E-mail: yth@dlut.edu.cn
[a]Associate Professor
[b]Ph.D. Candidate
[c]Professor

ISSN: 1225-4568 (Print), 1598-6217 (Online)

eigenvectors. Magalhaes *et al*. (2009) mentioned that stabilization diagram is the most popular approach to separate the physical and spurious modes by checking the stable points in consistent frequency. Verboven *et al*. (2002) presented a criteria about the complexity of modal vectors to distinguish the spurious modes. Bazan (2004) analyzed the sensitivity of poles and provided estimates for the pole error in the ERA. Cara *et al.* (2012) presented expectation maximization algorithm to identify modes with the parameters estimated by SSI, which is useful to discard the spurious modes. Marchesiello *et al*. (2016) investigated on the effect of spurious poles on nonlinear dynamics. However, there are still some problems for stabilization diagram and the singular value treatment. Due to the noises, it is hard to decide which consistent frequency contains most stable points in the stabilization diagram. On the other hand, the noises can generate large singular values into real singular value, which is difficult to be distinguished.

To distinguish the spurious modes clearly, this paper presents an improved stabilization diagram method in the ERA, which adds a moving data diagram process after stabilization diagram to determine which mode is spurious. This paper is organized as follows. Section 2 reviews the ERA and stabilization diagram method. Section 3 proved that the ERA can be performed by any choice of two Hankel matrices with one time step shift. Then the proposed moving data diagram is presented, where the noise effect on eigenvalues is analyzed. Finally, the proposed method is proved by a numerical example.

2. Eigensystem realization algorithm and stabilization diagram

2.1 Eigensystem realization algorithm

In order to present clearly the spurious mode identification problem, first the ERA (Juang and Pappa 1985) and the stabilization diagram (Peeters and Roeck 2001) are reviewed briefly, which would be used in the next section discussion. The ERA is performed under the condition of impulse input. The formulation of the free pulse response is utilized to deduce the state matrix.

Considering an n degree-of-freedom (DOF) system, the dynamics in discrete time domain is

$$\mathbf{x}_{k+1} = \mathbf{A}\mathbf{x}_k + \mathbf{B}\mathbf{u}_k \tag{1}$$

$$\mathbf{y}_k = \mathbf{C}\mathbf{x}_k + \mathbf{D}\mathbf{u}_k \tag{2}$$

where k means k-th time step; $\mathbf{A}$, $\mathbf{B}$, $\mathbf{C}$, $\mathbf{D}$ are state matrix, input matrix, output matrix and feed-through matrix in discrete time domain, respectively; $\mathbf{x}_k$, $\mathbf{y}_k$, $\mathbf{u}_k$ are state vector, output measurement vector and input vector, respectively.

For the impulse input, which means $\mathbf{u}_0$=1 and $\mathbf{u}_k$=0, ($k\neq0$), the response (Markov parameters) can be expressed as

$$\mathbf{y}_k = \mathbf{C}\mathbf{A}^{k-1}\mathbf{B},\ (k \geq 1) \tag{3}$$

The above Markov parameters can form the Hankel matrix as follows

$$\mathbf{H}(k-1) = \begin{pmatrix} \mathbf{C} \\ \mathbf{CA} \\ \cdots \\ \mathbf{CA}^{p-1} \end{pmatrix} \mathbf{A}^{k-1} \begin{pmatrix} \mathbf{B} & \mathbf{AB} & \cdots & \mathbf{A}^{k+q-1}\mathbf{B} \end{pmatrix} = \mathbf{O}_p \mathbf{A}^{k-1} \mathbf{C}_q \tag{4}$$

where $\mathbf{O}_p$,$\mathbf{C}_q$ are the observability and controllability matrices, respectively.

The ERA always using the Hankel matrices $\mathbf{H}(0)$ and $\mathbf{H}(1)$ (Juang and Pappa 1985). $\mathbf{H}(0)$ can be decomposed by singular value decomposition (SVD) as follows:

The ERA always using the Hankel matrices $\mathbf{H}(0)$ and $\mathbf{H}(1)$ (Juang and Pappa 1985). $\mathbf{H}(0)$ can be decomposed by singular value decomposition (SVD) as follows

$$\mathbf{H}(0) = \mathbf{O}_p \mathbf{C}_q = \mathbf{U}\boldsymbol{\Gamma}^2 \mathbf{V}^{\mathrm{T}} \tag{5}$$

$\mathbf{H}(1)$ has the state matrix $\mathbf{A}$ more than $\mathbf{H}(0)$, so the state matrix $\mathbf{A}$ can be calculated by $\mathbf{O}_p$ and $\mathbf{C}_q$. After setting $\mathbf{P} = \mathbf{U}\boldsymbol{\Gamma}$ and $\mathbf{Q} = \boldsymbol{\Gamma}\mathbf{V}^{\mathrm{T}}$, $\mathbf{H}(1)$ can be also expressed as follows

$$\mathbf{H}(1) = \mathbf{O}_p \mathbf{A} \mathbf{C}_q = \mathbf{P}\hat{\mathbf{A}}\mathbf{Q} \tag{6}$$

It can be proved that both $\mathbf{A}$ and $\hat{\mathbf{A}}$ are minimal realization, which means that they have the same eigenvalues (Jeffrey 1998). Therefore, $\hat{\mathbf{A}}$ can be solved simply.

$$\hat{\mathbf{A}} = \boldsymbol{\Gamma}^{-1}\mathbf{U}^T \mathbf{H}(1) \mathbf{V}\boldsymbol{\Gamma}^{-1} \tag{7}$$

Then, the eigenvectors $\boldsymbol{\psi}$ and eigenvalues $\mathbf{z}^d$ for the state matrix $\hat{\mathbf{A}}$ can be obtained. The eigenvalue for j-th mode in continuous time domain is

$$s_j = \ln z_j^d / \Delta t = s_{re,j} + s_{im,j} i \tag{8}$$

where Δt is the sampling time.

The natural frequency f_j is the absolute value of the eigenvalue in Eq.(8). The damping ratio ζ_j is the real part divided by the absolute value in Eq.(8). The mode shapes is described as (Juang and Pappa 1985)

$$\boldsymbol{\Phi} = \mathbf{E}_p^{\mathrm{T}} \mathbf{P} \boldsymbol{\Gamma} \boldsymbol{\psi} \tag{9}$$

$$\mathbf{E}_p = [\mathbf{I}, \mathbf{0}, \ldots \mathbf{0}] \tag{10}$$

2.2 Stabilization diagram

The stabilization diagram has two axes, the frequency axis and order axis, which illustrates the stability of frequency with the different order (Peeters and Roeck 2001). In the ERA, the order axis describes the changing order (rank) of $\boldsymbol{\Gamma}^2$ for SVD of Hankel matrix or the changing order (rank) of Hankel matrix in Eq. (5).

Due to the noises in the measurement, the singular values $\boldsymbol{\Gamma}^2$ have large rank which contains the noise singular value. The noise singular value can introduce the spurious modes which are hardly distinguished. The stabilization diagram surveys the stability of the identified frequencies

by changing different order of $\mathbf{\Gamma}^2$ which can be achieved by truncation. If the frequency is not changed for different order of $\mathbf{\Gamma}^2$, it means that the frequency is stable. However, the noises can generate the stable frequency, whose corresponding damping ratio and mode are instable. So the stable points in stabilization diagram can be decided by the stability of identified frequencies, damping ratios and modes.

To plot the stabilization diagram for the ERA, three kind of parameters, the frequencies s_j in Eq. (8), the damping ratio ζ_j and mode shapes in Eq. (9), should be calculated first. The errors between two different truncated order n_{t1} and n_{t2} for the three kind of parameters are denoted as

$$e_s = \left(s_{j,n_{t2}} - s_{j,n_{t1}}\right) / s_{j,n_{t1}} \tag{11}$$

$$e_\zeta = \left(\zeta_{j,n_{t2}} - \zeta_{j,n_{t1}}\right) / \zeta_{j,n_{t1}} \tag{12}$$

$$\mathrm{MAC} = \left|\boldsymbol{\varphi}^*_{j,n_{t1}} \boldsymbol{\varphi}_{j,n_{t2}}\right| / \sqrt{\left|\boldsymbol{\varphi}^*_{j,n_{t1}} \boldsymbol{\varphi}_{j,n_{t1}}\right| \left|\boldsymbol{\varphi}^*_{j,n_{t2}} \boldsymbol{\varphi}_{j,n_{t2}}\right|} \tag{13}$$

$$\mathrm{DMAC} = 1 - \mathrm{MAC} \tag{14}$$

where | | is the absolute value; * is the transpose complex conjugate; $\boldsymbol{\varphi}_j$ is j-th mode and the j-th vector of $\mathbf{\Phi}$ in Eq. (9); MAC represents the meaning of modal assurance criterion; DMAC means deducted modal assurance criterion.

If the following equations are satisfied, the points are stable and can be plotted in the stabilization diagram.

$$e_s \le e_{s,\lim} \tag{15}$$

$$e_s \le e_{s,\lim} \tag{16}$$

$$\mathrm{DMAC} \le e_{\mathrm{DMAC},\lim} \tag{17}$$

where $e_{s,\lim}$, $e_{\zeta,\lim}$ and $e_{\mathrm{DMAC},\lim}$ are the error limit values for frequency, damping ratio and mode shape, respectively. After the stable points are plotted in the stabilization diagram, the system final stable frequencies can be chosen as the frequency which has more stable points. Then, the damping ratios and mode shapes can be calculated by the chosen frequencies.

During the process of Eq. (15), many spurious modes can be distinguished. However, there are still some spurious modes displayed as spurious stable points in stabilization diagram. Sometimes, there are many spurious stable points such that the stable frequencies cannot be picked out. Therefore, the stabilization diagram still cannot distinguish the spurious modes effectively.

3. Improved stabilization diagram

In this section, the stabilization diagram is improved by adding additional process, which fixes the order of singular value matrix for Hankel matrix and varies the choice of two Hankel matrix with one time step shift to replace $\mathbf{H}_{pq}(0)$ and $\mathbf{H}_{pq}(1)$ in Eqs. (5) and (6). The effectiveness of this process to distinguish spurious modes would be studied and illustrated in the following.

As described in section 2.1, the choice of two Hankel matrices are defined as

$$\mathbf{H}(k-1) = \mathbf{P}\mathbf{A}^{k-1}\mathbf{Q} \tag{18}$$

$$\mathbf{H}(k) = \mathbf{P}\mathbf{A}^{k}\mathbf{Q} \tag{19}$$

The SVD for Eq. (18) is expressed as

$$\mathbf{H}(k-1) = \mathbf{P}\mathbf{T}\mathbf{T}^{-1}\mathbf{A}^{k-1}\mathbf{R}^{-1}\mathbf{R}\mathbf{Q} = \mathbf{U}\mathbf{\Gamma}^2\mathbf{V}^{\mathrm{T}} \tag{20}$$

where

$$\mathbf{U} = \mathbf{P}\mathbf{T} \tag{21}$$

$$\mathbf{V} = \mathbf{Q}^{\mathrm{T}}\mathbf{R}^{\mathrm{T}} \tag{22}$$

$$\mathbf{\Gamma}^2 = \mathbf{T}^{-1}\mathbf{A}^{k-1}\mathbf{R}^{-1} \tag{23}$$

$$\mathbf{U}^{\mathrm{T}}\mathbf{U} = (\mathbf{P}\mathbf{T})^{\mathrm{T}}\,\mathbf{P}\mathbf{T} = \mathbf{T}^{\mathrm{T}}\mathbf{P}^{\mathrm{T}}\mathbf{P}\mathbf{T} = 1 \tag{24}$$

$$\mathbf{V}^{\mathrm{T}}\mathbf{V} = \mathbf{R}\mathbf{Q}(\mathbf{R}\mathbf{Q})^{\mathrm{T}} = \mathbf{R}\mathbf{Q}\mathbf{Q}^{\mathrm{T}}\mathbf{R}^{\mathrm{T}} = 1 \tag{25}$$

As Eq. (7) process, $\mathbf{H}(k)$ is left-multiplied by $\mathbf{U}^{\mathrm{T}}$ and right-multiplied by $\mathbf{V}$.

$$\mathbf{U}^{\mathrm{T}}\mathbf{H}(k)\mathbf{V} = \mathbf{U}^{\mathrm{T}}\mathbf{P}\mathbf{A}^{k}\mathbf{Q}\mathbf{V} = \mathbf{T}^{\mathrm{T}}\mathbf{P}^{\mathrm{T}}\mathbf{P}\mathbf{T}\mathbf{T}^{-1}\mathbf{A}^{k}\mathbf{R}^{-1}\mathbf{R}\mathbf{Q}\mathbf{Q}^{\mathrm{T}}\mathbf{R}^{\mathrm{T}} \tag{26}$$

Due to Eqs. (21)-(25), both sides of Eq. (26) multiplying $\mathbf{\Gamma}^{-1}$ can obtain

$$\begin{aligned}\mathbf{\Gamma}^{-1}\mathbf{U}^{\mathrm{T}}\mathbf{H}(k)\mathbf{V}\mathbf{\Gamma}^{-1} &= \mathbf{\Gamma}^{-1}\mathbf{T}^{-1}\mathbf{A}^{k-1}\mathbf{R}^{-1}\mathbf{R}\mathbf{A}\mathbf{R}^{-1}\mathbf{\Gamma}^{-1} \\ &= \mathbf{\Gamma}\mathbf{R}\mathbf{A}\mathbf{R}^{-1}\mathbf{\Gamma}^{-1} = \hat{\mathbf{A}}\end{aligned} \tag{27}$$

where $\hat{\mathbf{A}}$ is also minimization realization state matrix which has the same eigenvalue of $\mathbf{A}$.

Therefore, it is obvious that the SVD of $\mathbf{H}(k-1)$ can be used into $\mathbf{H}(k)$ to get the minimization realization state matrix.

When there exists noise in the measurement, Eqs. (18) and (19) is changed to

$$\mathbf{H}(k-1) = \mathbf{P}\mathbf{A}^{k-1}\mathbf{Q} + \mathbf{\Delta}_{k-1} = \mathbf{P}_{k-1}\mathbf{A}_{k-1}^{k-1}\mathbf{Q}_{k-1} \tag{28}$$

$$\mathbf{H}(k) = \mathbf{P}\mathbf{A}^{k}\mathbf{Q} + \mathbf{\Delta}_{k} = \mathbf{P}_{k}\mathbf{A}_{k}^{k}\mathbf{Q}_{k} \tag{29}$$

where $\mathbf{P}$, $\mathbf{A}$, $\mathbf{Q}$ are real matrix without the effect of noises; $\mathbf{P}_{k\text{-}1}$ (or $\mathbf{P}_{k\text{-}1}$) and $\mathbf{P}_{k\text{-}1}$ (or $\mathbf{P}_k$) are the matrix polluted by noise $\mathbf{\Delta}_{k\text{-}1}$ (or $\mathbf{\Delta}_k$).

Then Eqs. (20) and (27) are changed to

$$\begin{aligned}\mathbf{H}(k-1) &= \mathbf{P}_{k-1}\mathbf{T}_{k-1}\mathbf{T}_{k-1}^{-1}\mathbf{A}_{k-1}^{k-1}\mathbf{R}_{k-1}^{-1}\mathbf{R}_{k-1}\mathbf{Q}_{k-1} \\ &= \mathbf{U}_{k-1}\mathbf{\Gamma}_{k-1}^2\mathbf{V}_{k-1}^{\mathrm{T}}\end{aligned} \tag{30}$$

$$\begin{aligned}&\mathbf{\Gamma}_{k-1}^{-1}\mathbf{U}_{k-1}^{\mathrm{T}}\mathbf{H}(k)\mathbf{V}_{k-1}\mathbf{\Gamma}_{k-1}^{-1} = \mathbf{\Gamma}_{k-1}^{-1}\left(\mathbf{T}_{k-1}^{\mathrm{T}}\mathbf{P}_{k-1}^{\mathrm{T}}\mathbf{P}_k\mathbf{T}_{k-1}\right) \\ &\times\left(\mathbf{T}_{k-1}^{-1}\mathbf{A}_k^{k-1}\mathbf{R}_{k-1}^{-1}\right)\mathbf{R}_{k-1}\mathbf{A}_k\mathbf{R}_{k-1}^{-1}\left(\mathbf{R}_{k-1}\mathbf{Q}_k\mathbf{Q}_{k-1}^{\mathrm{T}}\mathbf{R}_{k-1}^{\mathrm{T}}\right)\mathbf{\Gamma}_{k-1}^{-1}\end{aligned} \tag{31}$$

where the matrix with the subscript k-1 is from the Hankel matrix $\mathbf{H}(k-1)$; so is the matrix with subscript k. The parts

in the brackets in Eq. (31) are assumed as

$$\mathbf{T}_{k-1}^{\mathrm{T}}\mathbf{P}_{k-1}^{\mathrm{T}}\mathbf{P}_k\mathbf{T}_{k-1}=\mathbf{T}_{k-1}^{\mathrm{T}}\mathbf{P}_{k-1}^{\mathrm{T}}\mathbf{P}_{k-1}\mathbf{T}_{k-1}=\mathbf{I} \tag{32}$$

$$\mathbf{R}_{k-1}\mathbf{Q}_k\mathbf{Q}_{k-1}^{\mathrm{T}}\mathbf{R}_{k-1}^{\mathrm{T}}=\mathbf{R}_{k-1}\mathbf{Q}_{k-1}\mathbf{Q}_{k-1}^{\mathrm{T}}\mathbf{R}_{k-1}^{\mathrm{T}}=\mathbf{I} \tag{33}$$

$$\mathbf{T}_{k-1}^{-1}\mathbf{A}_k^{k-1}\mathbf{R}_{k-1}^{-1}=\mathbf{T}_{k-1}^{-1}\mathbf{A}_{k-1}^{k-1}\mathbf{R}_{k-1}^{-1}=\mathbf{\Gamma}_{k-1}^2 \tag{34}$$

where the letter "**I** " represents the identity matrix. Then Eq .(31) is equal to

$$\mathbf{\Gamma}_{k-1}^{-1}\mathbf{U}_{k-1}^{\mathrm{T}}\mathbf{H}(k)\mathbf{V}_{k-1}\mathbf{\Gamma}_{k-1}^{-1}=\mathbf{\Gamma}_{k-1}\mathbf{R}_{k-1}\mathbf{A}_k\mathbf{R}_{k-1}^{-1}\mathbf{\Gamma}_{k-1}^{-1}=\hat{\mathbf{A}}_k \tag{35}$$

It means that the SVD of **H**(*k*−1) with noise $\mathbf{\Delta}_{k-1}$ can be used into **H**(*k*) with noise $\mathbf{\Delta}_k$ to get the similar state matrix with the assumption Eqs. (32)-(34).

From Eqs. (28) and (29), the noise matrix $\mathbf{\Delta}_{k-1}$ is split into the real matrix **P**, $\mathbf{A}^{k-1}$, **Q** to form $\mathbf{P}_{k-1}$, $\mathbf{A}_{k-1}^{k-1}$, $\mathbf{Q}_{k-1}$. $\mathbf{\Delta}_k$ is split into **P**, $\mathbf{A}^k$, **Q** to form $\mathbf{P}_k$, $\mathbf{A}_k^k$, $\mathbf{Q}_k$. The differences of the real matrices from **H**(*k*−1) and **H**(*k*) are $\mathbf{A}_{k-1}^{k-1}$ and $\mathbf{A}_k^k$. Therefore, it is reasonable that $\mathbf{P}_k$ and $\mathbf{Q}_k$ are equal to $\mathbf{P}_{k-1}$ and $\mathbf{Q}_{k-1}$, respectively, which can be convenient for the following investigation. So Eqs.(32) and (33) can be satisfied.

The noise matrices $\mathbf{\Delta}_{k-1}$ and $\mathbf{\Delta}_k$ can be recognized as the same matrix. When $\mathbf{P}_k$=$\mathbf{P}_{k-1}$ and $\mathbf{Q}_k$=$\mathbf{Q}_{k-1}$, the power of matrix **A** in **H**(*k*−1) and **H**(*k*) are *k*-1 and *k*, which makes that the noise matrix split into **A** are different and can be expressed as

$$\mathbf{A}_{k-1}=\mathbf{A}+\boldsymbol{\delta}_{\mathbf{A}_{k-1}} \tag{36}$$

$$\mathbf{A}_k=\mathbf{A}+\boldsymbol{\delta}_{\mathbf{A}_k} \tag{37}$$

When *k* is large, according to $\mathbf{A}_{k-1}^{k-1}$ or $\mathbf{A}_k^k$, $\mathbf{\Delta}_{k-1}$ or $\mathbf{\Delta}_k$ would be square root (or split) many times, which causes $\boldsymbol{\delta}_{\mathbf{A}_k}$ is equal to $\boldsymbol{\delta}_{\mathbf{A}_{k-1}}$. Then, A_k is equal to A_{k-1}, which means that Eq. (34) is satisfied. So, along with raising value of *k*, all the obtained $\hat{\mathbf{A}}_k$ are similar matrices and have same eigenvalues. However, in the other way, when *k* is not large enough, $\hat{\mathbf{A}}_k$ with different *k* are not similar matrices and do not have same eigenvalues. Simply, the above discussion can be described as

$$\begin{cases}\hat{\mathbf{A}}_k\sim\hat{\mathbf{A}}_{k-1}, & k \text{ is large enough}\\ \hat{\mathbf{A}}_k\tilde{\neq}\hat{\mathbf{A}}_{k-1}, & k \text{ is small}\end{cases} \tag{38}$$

where the symbol "~" means that two matrices are similar; the symbol "$\tilde{\neq}$" is not similar; $\hat{\mathbf{A}}_{k-1}$ is obtained as the procedure in Eqs. (30) and (35) using **H**(*k*−2) and **H**(*k*−1). It is obvious that the property of eigenvalue changing with different *k* can be utilized to distinguish whether the eigenvalue is affected by noise or not. If the eigenvalue is not changed a lot along *k* rising, it means that the noise does not affect the eigenvalue too much. While the eigenvalue is varying obviously, it means that the noise affects the eigenvalue a lot. Then *k* is still rising, and the eigenvalue should be stable, which means that the eigenvalue has been all polluted by noise.

Another important topic is the choice of the truncated order of the singular matrix $\mathbf{\Gamma}_k$. $\mathbf{\Gamma}_k$ can be rewritten as

$$\begin{aligned}\mathbf{\Gamma}_k &= diag\left(l_1,l_2\ldots l_{2n},l_{2n+1}\ldots l_{n_t}\ldots l_H\right)\\ &= diag\left(l_{0,1}+\delta_1,l_{0,2}+\delta_2\ldots l_{0,2n}+\delta_{2n},\delta_{2n+1}\ldots\delta_{n_t}\ldots\delta_H\right)\end{aligned} \tag{39}$$

where l_i (*i*=1…*H*) is the *i*-th order singular value of $\mathbf{\Gamma}_k$; 2*n* is the real singular order; n_t is the truncated order; H is the minimization of the row and column number of **H**(*k*); $l_{0,i}$ (*i*=1…2*n*) is the *i*-th order real singular value of $\mathbf{\Gamma}$, which satisfies $l_{0,i}\geq l_{0,i+1}$; δ_i $(i=1\ldots H)$ is the noise effect on each singular value. From Eq. (39), it should be known that when *i*>2*n*, the singular value of $\mathbf{\Gamma}_k$ is caused by noise, and the real singular value is 0.

Due to $l_{0,i}\geq l_{0,i+1}$, when *i* is very small, $l_{0,i}$ is much larger than δ_i. Then from Eq. (35), the *i*-th eigenvalue of $\hat{\mathbf{A}}_k$ will not change a lot by noise. While *i* is closed to 2*n*, $l_{0,j}$ is hardly distinguished with δ_i. So when *i* is near 2*n*, $l_{0,i}$ will be polluted more and more with rising *k*. According to Eq. (35), the *i*-th eigenvalue would vary a lot along rising *k*. For the case *i*>2*n*, all the singular value l_i is caused by noise. The eigenvalue of $\hat{\mathbf{A}}_k$ will also not changed a lot.

Therefore, the choice of the truncated order n_i of $\mathbf{\Gamma}_{k-1}^2$ in Eq. (30) is a big issue. When the order n_i is too high, the noise singular values in $\mathbf{\Gamma}_{k-1}^2$ will be introduced. It would bring out a consequence that the higher order eigenvalue of $\hat{\mathbf{A}}_k$ is also not changed too much. Therefore, the stabilization diagram mentioned in section 2.2 should be used first to decide the concerned order of singular values. If the concerned order is chosen as n_i, then **U**, **Γ**, **V** in Eq. (20) are truncated as Eqs. (40)-(42).

$$\mathbf{U}_{n_t}=\mathbf{U}_{k-1}(:,1:n_t) \tag{40}$$

$$\mathbf{V}_{n_t}=\mathbf{V}_{k-1}(:,1:n_t) \tag{41}$$

$$\mathbf{\Gamma}_{n_t}=\mathbf{\Gamma}_{k-1}(1:n_t,1:n_t) \tag{42}$$

Then the order n_i is fixed and the power *k* is changed, which is used to check whether the eigenvalue of $\hat{\mathbf{A}}_k$ is stable or not. The procedure can be summarized as shown in Fig. 1.

4. Numerical example

In order to prove the propose method, a numerical example is investigated. To illustrate the spurious mode problem clearly, the example is revised from the reference (Qu *et al.* 2017) simulation example to be 8 DOF in-plane lumped-mass model. The mass and stiffness for each floor are list in Table 1. It should be noted that the structural damping employs the Rayleigh damping, which utilizes first two damping ratios to construct the damping matrix.

The example structure is excited by an impulse at the

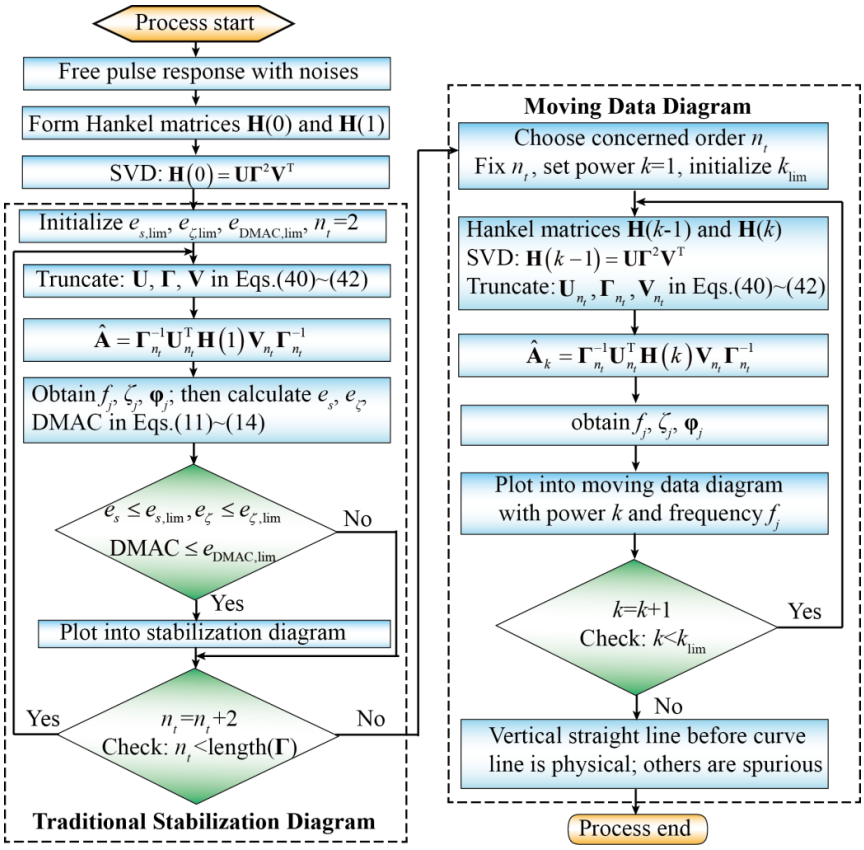

Fig. 1 Flow chart of the improved stabilization diagram

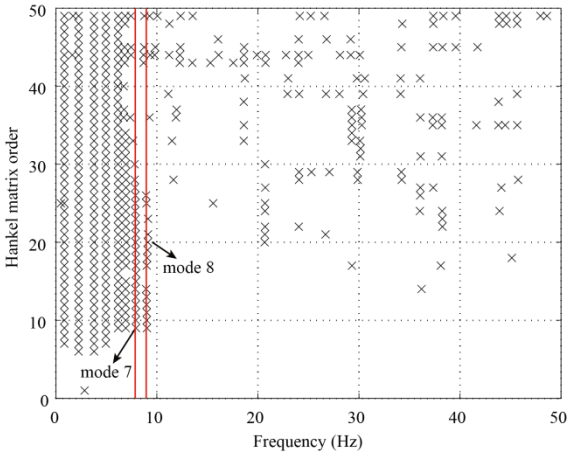

Fig. 2 Traditional stabilization diagram for k=1

Table 1 Model parameters

Floor No.	1	2~5	6~8
Mass ($\times 10^6$ kg)	1.126	1.100	1.100
Stiffness ($\times 10^6$N/m)	862.07	862.07	554.17
Damping	Rayleigh damping with first two damping ratios are 5%		

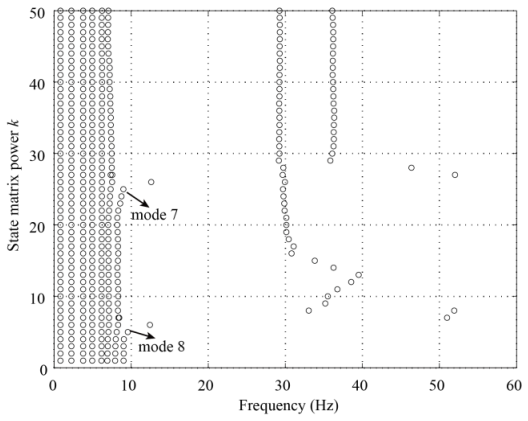

Fig. 3 Moving data diagram for n_t=16

beginning time. The sensors are supposed to collect the relative displacements for all the floors. The measurement noises are assumed to be 20% of the variance for the structural free pulse response. First, k is set to be 1. $e_{s,\mathrm{lim}}$, $e_{\zeta,\mathrm{lim}}$ and $e_{\mathrm{DMAC,lim}}$ in Eq. (15) are set to be 0.01, 0.05 and 0.02, respectively. According to the flowchart in Fig. 1, the traditional stabilization diagram can be drawn as shown in Fig. 2.

In Fig. 2, the symbol "× " means that the points with the corresponding frequency s_j, damping ζ_j and DMAC are satisfied Eq. (15). It is obvious that there are almost 8 stable modes, where mode 7 and mode 8 may not be physical modes. To verify it, moving data diagram is implemented after determining the truncated order n_t. From Fig. 2, there are 8 modes concerned. So n_t is set to 16, and the moving data diagram is executed as shown in Fig. 3 following flowchart Fig. 1.

From Fig. 3, it is founded that mode 7 is affected when k is larger, while mode 8 is almost polluted at the beginning. Along k is rising, the points are not stable, which means that

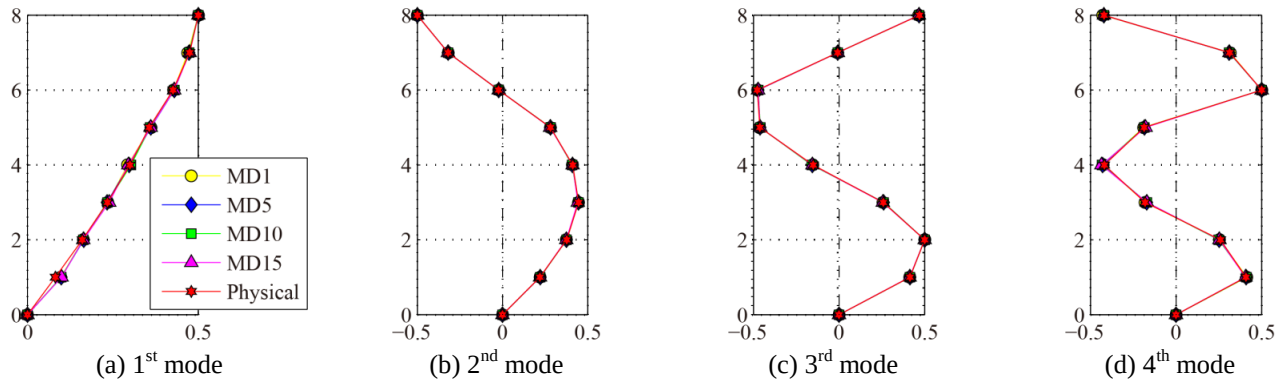

(a) 1st mode (b) 2nd mode (c) 3rd mode (d) 4th mode

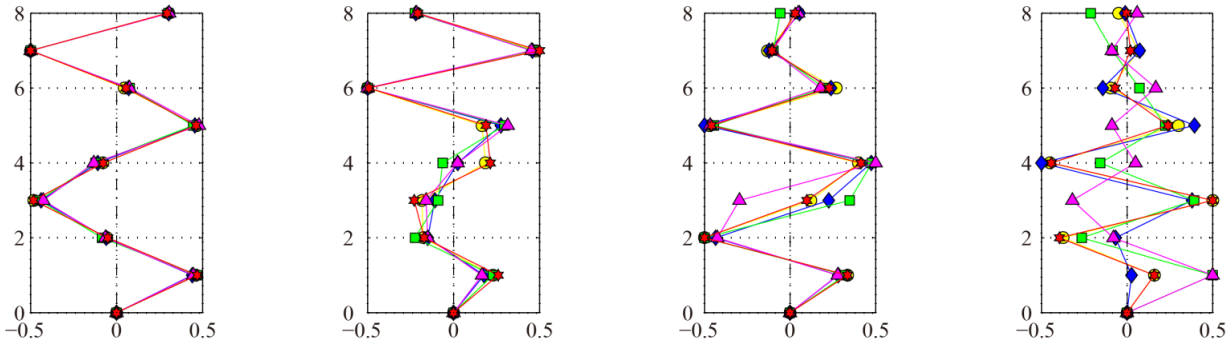

(e) 5th mode (f) 6th mode (g) 7th mode (h) 8th mode

Fig. 4 Mode comparisons with different *k*

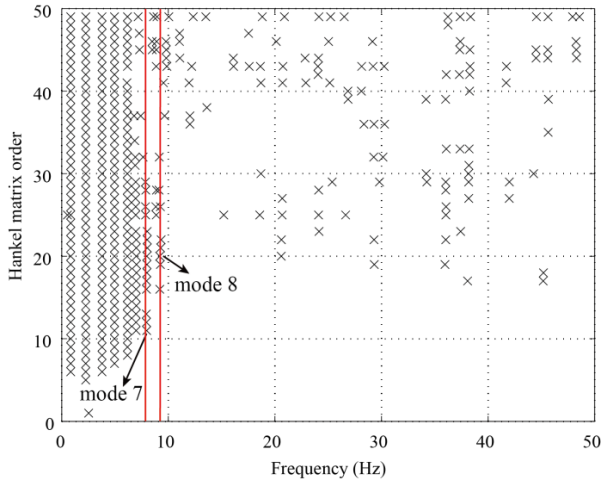

Fig. 5 Traditional stabilization diagram for *k*=5

the noises introduce spurious modes. To display the spurious modes, the mode comparisons are shown in Fig. 4.

In Fig. 4, all the modes are identified with the truncated order n_t, which is concerned order determined by tradition stabilization diagram in Fig. 2. Figs. 4(a)-(h) represent the 1st mode to 8th mode. In Fig. 4(i), the legend "MD1" means "Moving Data" diagram for *k*=1. So "MD5", "MD10" and "MD15" are for *k*=5, *k*=10 and *k*=15. The red color modes are the physical modes. It is obvious that Figs. 4(a)~(e) (1st to 5th modes) are almost not affected by noises. From Figs. 4(f)-(h), it is found that the green modes, purple modes and blue modes have more difference than the yellow and red ones. It means that along rising power *k*, the modes can be polluted more easily. The yellow modes are a little different with the red ones, which means that even for *k*=1, the modes can be affected a little. From Fig. 4(f), the difference of different color modes illustrates that the 6th mode is a little spurious. For Figs. 4 (g)-(h), especially Fig. 4(h), the modes with different colors are so different, which means that 7th mode and 8th mode are spurious modes and not suggested to be used.

It should be noted that although the yellow modes are closed to physical modes, it is hard to measure the response at the beginning time point. If the response from the 5th time point is measured, which means *k*=5, the stabilization diagram is plotted in Fig. 5.

It is obvious that Fig. 5 is similar to Fig. 2, where the 7th and 8th modes are still not to be sure the physical modes. To study the MAC values in Eq. (11), Fig. 6 is drawn.

From Fig. 6(a)-(d), it is obvious that the 6th~7th modes are affected by noises, especially for 7th mode and 8th mode. From the moving data diagram in Fig. 3, the 6th mode is a little not a straight line, which shows that the 6th mode is already affected. Therefore, the moving data diagram in Fig. 3 can distinguish which mode is spurious mode that is not suggested to be used.

It should be noted that the proposed method is only available for the free decayed response. If the excitation is ambient with white property, the free decayed response should be first obtained by some well-known method, such as NExT or RDT.

5. Conclusions

The noises in measurement can cause the spurious modes through modal identification method, which is hardly divided. This paper proposes an improved

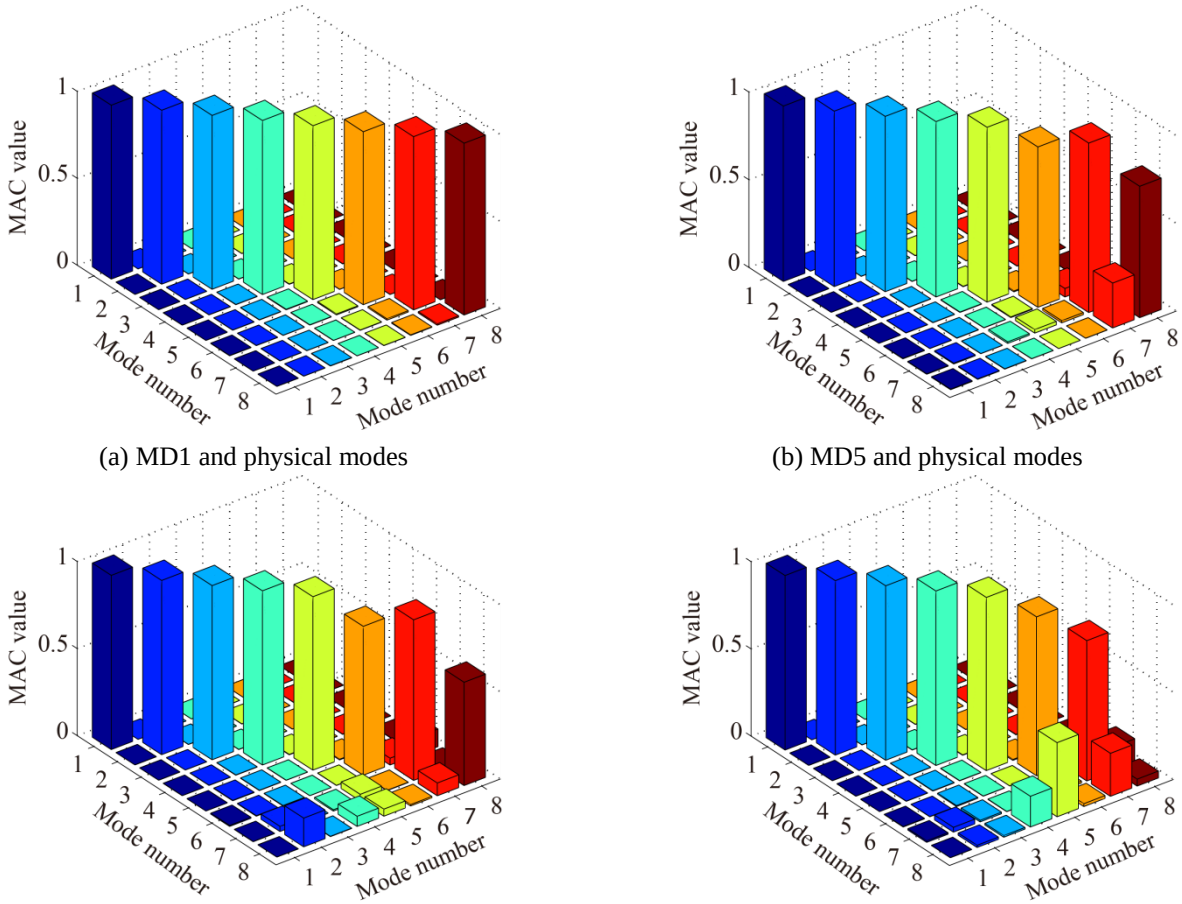

(a) MD1 and physical modes

(b) MD5 and physical modes

(c) MD10 and physical modes

(d) MD15 and physical modes

Fig. 6 Mode values of all 8 modes with different k

stabilization diagram in the ERA for distinguishing spurious modes. With the method investigation and the case study, some conclusions are summarized as follows:

- The improved stabilization diagram in the ERA, which combines the proposed moving data diagram and the traditional stabilization diagram, is an efficient method for distinguishing spurious modes.
- The flowchart of proposed improved stabilization diagram in the ERA is summarized. The traditional stabilization diagram is first performed to determine the concerned truncated order n_t of Hankel matrix $\mathbf{H}(k-1)$. Then the proposed moving data diagram is implemented with the fixed truncated order n_t and rising the power k.
- An eight story numerical structure is used to prove the proposed method, and also demonstrate the efficacy of distinguishing spurious modes. The results shows that the higher modes are polluted more easily than the lower modes, and the more modes are polluted (or the more spurious modes are generated) with rising the power k.

Acknowledgements

This research work was jointly supported by the National Natural Science Foundation of China (Grant Nos. 51625802, 51778105), the 973 Program (Grant No. 2015CB060000), the Opening Funds of State Key Laboratory of Building Safety and Built Environment (Grant No. BSBE2016-01), and the Fundamental Research Funds for the Central Universities (Grant No. DUT16RC(3)011).

References

Au, S.K. and Zhang, F.L. (2016), "Fundamental two-stage formulation for Bayesian system identification, part I: general theory", *Mech. Syst. Signal. Pr.*, **66**, 31-42.

Bazan, F.S.V. (2004), "Eigensystem realization algorithm (ERA): reformulation and system pole perturbation analysis", *J. Sound Vib.*, **274**(1), 433-444.

Cara, F.J., Carpio, J., Juan, J. and Alarcon, E. (2012), "An approach to operational modal analysis using the expectation maximization algorithm", *Mech. Syst. Signal. Pr.*, **31**, 109-129.

Chen, H.P. and Maung, T.S. (2014), "Regularised finite element model updating using measured incomplete modal data", *J. Sound Vib.*, **333**(21), 5566-5582.

Ibraham, S.R. (2001), "Efficient random decrement computation for identification of ambient responses", *Proceedings of the 19th IMAC*, Orlando, FL.

James, G.H., Carne, T.G. and Lauffer, J.P. (1995), "The natural excitation technique (NExT) for modal parameter extraction from operating structures", *Modal. Anal.*, **10**(4), 260-277.

Jeffrey, B.B. (1998), *Linear optimal control: H2 and H-infinity methods*, Addison-Wesley Longman Publishing Co., Inc.

Juang, J.N. and Pappa, R.S. (1985), "An eigensystem realization

algorithm for modal parameter identification and model reduction", *J. Guid. Control. Dyn.*, **8**(5), 620-627.
Lei, Y., Sohn, H. and Yi, T.H. (2014), "Advances in monitoring-based structural identification, damage detection and condition assessment", *Struct. Stab. Dyn.*, **14**(5).
Li, H.N., Qu, C.X., Huo, L. and Nagarajaiah, S. (2016), "Equivalent bilinear elastic single degree of freedom system of multi-degree of freedom structure with negative stiffness", *J. Sound Vib*., **365**, 1-14.
Magalhaes, F., Cunha, A. and Caetano, E. (2009), "Online automatic identification of the modal parameters of a long span arch bridge", *Mech. Syst. Signal. Pr*., **23**(2), 316-329.
Marchesiello, S., Fasana, A. and Garibaldi, L. (2016), "Modal contributions and effects of spurious poles in nonlinear subspace identification", *Mech. Syst. Signal. Pr*., **74**, 111-132.
Peeters, B. and Roeck, G.D. (2001), "Stochastic system identification for operational modal analysis: a review", *J. Dyn. Syst.*, **123**(4), 659-667.
Qu, C.X., Li, H.N., Huo, L. and Yi, T.H. (2017), "Optimum value of negative stiffness and additional damping in civil structures", *J. Struct. Eng.*, 04017068.
Van Overschee, P. and De Moor, B.L. (2012), *Subspace Identification for Linear Systems: Theory-Implementation-Applications*, Springer Science & Business Media.
Verboven, P., Parloo, E., Guillaume, P. and Overmeire, M.V. (2002), "Autonomous structural health monitoring-part I: modal parameter estimation and tracking", *Mech. Syst. Signal. Pr.*, **16**(4), 637-657.
Yi, T.H., Li, H.N. and Gu, M. (2011), "A new method for optimal selection of sensor location on a high-rise building using simplified finite element model", *Struct. Eng. Mech.*, **37**(6), 671-684.
Yi, T.H., Li, H.N. and Zhang, X.D. (2012), "Sensor placement on Canton Tower for health monitoring using asynchronous-climb monkey algorithm", *Smart Mater. Struct.*, **21**(12), 125023.
Zhang, F.L. and Au, S.K. (2016), "Fundamental two-stage formulation for Bayesian system identification, part II: application to ambient vibration data", *Mech. Syst. Signal. Pr.*, **66**, 43-61.